iScience

CellPress
OPEN ACCESS

Article

Plasmodium sporozoite shows distinct motility patterns in responses to three-dimensional environments

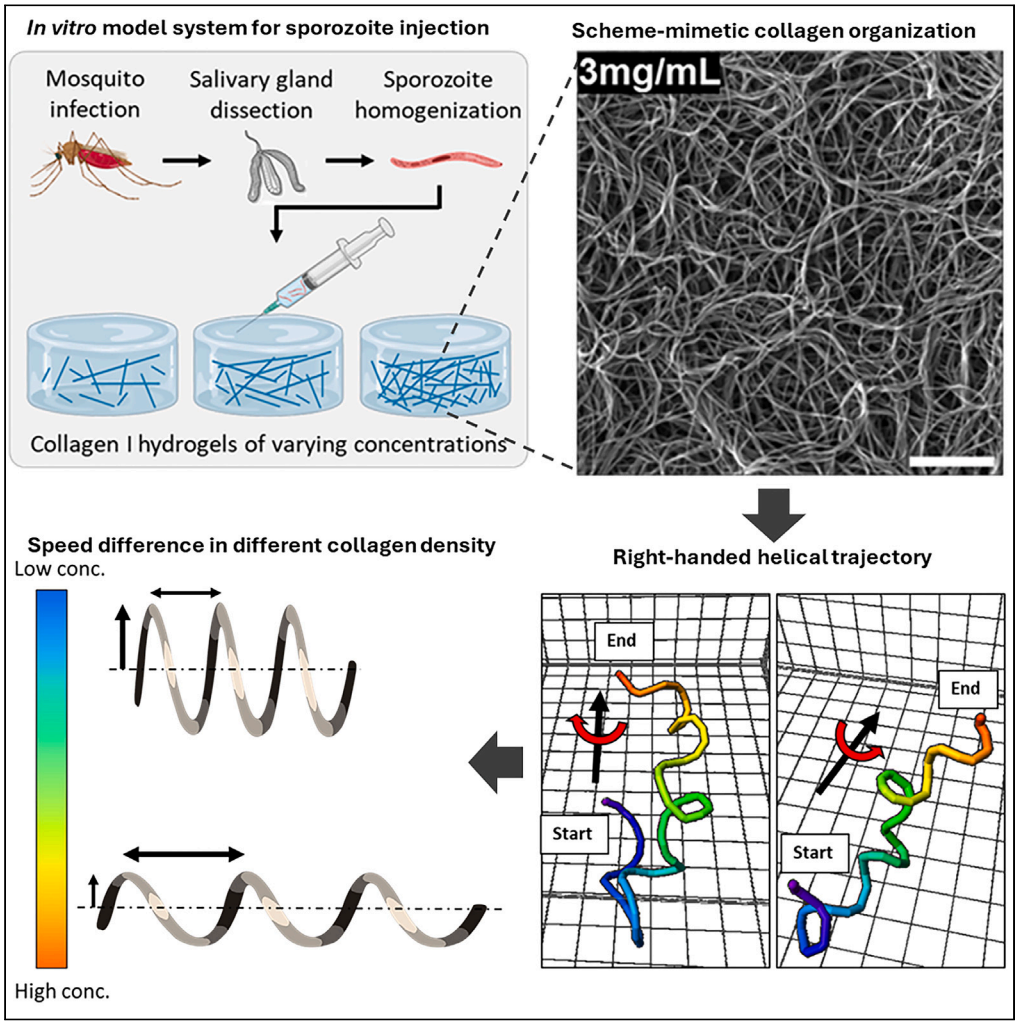

Zhenhui Liu, Songman Li, Pooja Anantha, ..., Abhai K. Tripathi, Yun Chen, Ishan Barman

atripat2@jhu.edu (A.K.T.)
yun.chen@jhu.edu (Y.C.)
ibarman@jhu.edu (I.B.)

Highlights

Collagen I hydrogel is a suitable *in vitro* 3D model to study sporozoite motility

Sporozoites exhibit right-handed helical trajectories migrating in collagen matrices

Sporozoites move faster in matrices of higher collagen concentrations

Liu et al., iScience *27*, 110463
August 16, 2024
https://doi.org/10.1016/j.isci.2024.110463

iScience

CellPress
OPEN ACCESS

Article

Plasmodium sporozoite shows distinct motility patterns in responses to three-dimensional environments

Zhenhui Liu,[1] Songman Li,[1] Pooja Anantha,[1] Tassanee Thanakornsombut,[2] Lintong Wu,[1] Junjie Chen,[1,3,4] Ryohma Tsuchiya,[1,3,4] Abhai K. Tripathi,[2,*] Yun Chen,[1,3,4,5,*] and Ishan Barman[1,*]

SUMMARY

During malaria infection, *Plasmodium* sporozoites, the fast-moving stage of the parasite, are injected by a mosquito into the skin of the mammalian host. In the skin, sporozoites need to migrate through the dermal tissue to enter the blood vessel. Sporozoite motility is critical for infection but not well understood. Here, we used collagen hydrogels with tunable fiber structures, as an *in vitro* model for the skin. After injecting sporozoites into the hydrogel, we analyzed their motility in three-dimension (3D). We found that sporozoites demonstrated chiral motility, in that they mostly follow right-handed helical trajectories. In high-concentration collagen gel, sporozoites have lower instantaneous speed, but exhibit straighter tracks compared to low-concentration collagen gel, which leads to longer net displacement and faster dissemination. Taken together, our study indicates an inner mechanism for sporozoites to adapt to the environment, which could help with their successful exit from the skin tissue.

INTRODUCTION

Malaria remains one of the most severe public health problems globally. There was an estimated 247 million cases of malaria and 619,000 deaths worldwide in 2021.[1] The disease is caused by the *Plasmodium* parasites, which are transmitted to the human host through a bite from an infected Anopheles mosquito. During blood meal, sporozoites, a highly motile stage of the parasite, are inoculated into the skin, where they need to migrate through the dermal tissue to enter the blood vessels. Through circulation, sporozoites reach the liver and invade hepatocytes to begin an exoerythrocytic stage of the parasite's life cycle. The skin stage is a significant bottleneck as only 10–100 sporozoites are inoculated by a mosquito bite,[2–7] of which only about 20% successfully enter blood circulation.[8,9] Sporozoites in search for blood vessels stay motile for up to 2 h in the dermis,[9] which makes sporozoites the longest extracellular stage of malaria parasites within the human host.[10,11] Therefore, the skin stage represents an attractive target for the development of prophylactics, and further understanding of the mechanisms that mediate sporozoite motility is an important prerequisite.[12–17]

Plasmodium, along with other *Apicomplexa*, have a unique way of locomotion referred to as gliding motility.[18–20] Unlike other types of cell migration such as flagellar propulsion, mesenchymal migration, or ameboid migration, the gliding motility does not require any protrusions from the cell or change in cell shape.[19] Gliding motility has been observed in different stages of *Plasmodium* parasites including sporozoites, ookinetes, and merozoites,[21,22] which is considered to be powered by the actomyosin motor that drives the posterior translocation of adhesins binding to the substrate, and in turn, propels the parasite forward.[19,23] Fast-moving characteristics of sporozoites are critical for the exit of parasites from the skin and finding a blood vessel,[24] and efforts have been made to characterize their motility. *In vivo* studies involve inoculating and imaging fluorescent sporozoites in the skin of mice.[8,10,13,25] Amino et al. first described that sporozoites exhibit two types of motility,[8] which was later confirmed by Hopp and colleagues.[9] Away from blood vessels, they move at high speed with greater mean squared displacement, whereas in the vicinity of blood vessels, they slow down and display circular motion. The authors observed that the curvature of sporozoite tracks engages with vasculature to optimize contact with dermal capillaries.[10] On the other hand, Hellmann et al. found that sporozoite movement patterns vary in different skin environments, in that the sporozoites inoculated in the tail skin followed straighter paths compared to those in the ear.[25] Both studies indicate the microenvironment plays an important role in regulating the sporozoite motility. However, the *in vivo* microenvironment is complex, making it difficult to dissect the role of individual components within the dermal matrix.

In vitro models such as two-dimensional (2D) and three-dimensional (3D) substrates, on the other hand, are a practical way to investigate sporozoite motility in a more controlled environment. Sporozoites are known to move in counterclockwise circles on a 2D glass surface. They

[1]Department of Mechanical Engineering, Johns Hopkins University, Baltimore, MD, USA
[2]Department of Molecular Microbiology & Immunology, Johns Hopkins University, Baltimore, MD, USA
[3]Institute for NanoBioTechnology, Johns Hopkins University, Baltimore, MD, USA
[4]Center for Cell Dynamics, Johns Hopkins University, Baltimore, MD, USA
[5]Lead contact
*Correspondence: atripat2@jhu.edu (A.K.T.), yun.chen@jhu.edu (Y.C.), ibarman@jhu.edu (I.B.)
https://doi.org/10.1016/j.isci.2024.110463

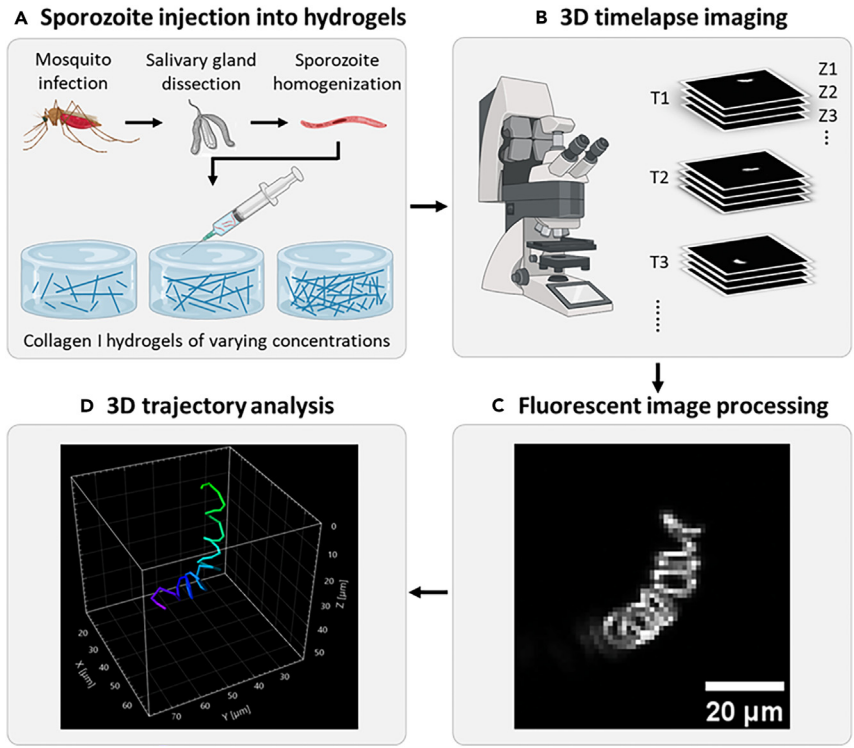

Figure 1. Schematics of the workflow for 3D sporozoite migration analysis

(A) Mosquitos were infected with *P. berghei*-mCherry, and the salivary glands were dissected and homogenized to extract the sporozoites. Sporozoites were then injected into collagen I hydrogels of different concentrations.

(B) Timelapse z stack images were acquired using a confocal microscope.

(C) Images were processed and (D) analyzed for sporozoite 3D motility.

move in a stick-slip manner using the formation and turnover of discrete adhesion sites.[26,51,52] Their chirality might be due to the polar rings and secretory organelles being tilted, allowing for the formation of adhesion with substrates on only one side.[26] In 3D hydrogels, sporozoites were observed to mostly move in helical trajectories,[27] and their movement is sensitive to the stiffness and porosity of the hydrogels.[22]

However, there are a few limitations in the existing *in vitro* studies. First, to date most of the *in vitro* studies were performed in hydrogels made of materials such as Matrigel or polyacrylamide.[22,28] These hydrogels, although providing valuable insights, do not necessarily fully represent the composition, microscale architecture, and mechanical properties of skin tissues, whose extracellular matrix is primarily made of collagen I. Second, images were either captured using a widefield microscope or first captured in several z stacks with a confocal microscope but then projected onto the X-Y plane for visualization and analysis,[22,29] thereby not providing the 3D perspective of sporozoite movement.

In this study, we introduced collagen-I-based hydrogels as the platform to study sporozoite locomotion. The fiber density and stiffness of the collagen I hydrogel can be tuned to represent the range of corresponding values found in the skins of different individuals. We injected *Plasmodium berghei* sporozoites expressing the fluorescent protein mCherry[10] (*P. berghei*-mCherry) into the hydrogel, mimicking the process of mosquito inoculation. Three-dimensional timelapse images were collected of sporozoites migrating within collagen using a confocal fluorescence microscope (Figure 1). Trajectory analysis revealed that sporozoites move in a helical path, with a dominant predisposition for right-handed chirality. The speed and the pattern of the helical path are highly dependent on the local availability of collagen fibers to the migrating sporozoite.

RESULTS

Collagen I hydrogels support continuous sporozoite motility

We used collagen I hydrogel, the main component of dermal extracellular matrix (ECM), as the model system to study the 3D motility of sporozoites. To determine the relation between sporozoite motility and collagen fiber structure, we first fabricated hydrogels of various collagen concentrations ranging from 1.5 to 6 mg/mL at various gelation temperatures.[30] After injection, *P. berghei*-mCherry sporozoites showed continuous motility in hydrogels of concentrations ranging from 3 to 6 mg/mL, which were cured at 37°C (Videos S1, S2, and S3). In contrast, sporozoites were immobile or frequently detached from the collagen fibers in 1.5 mg/mL collagen hydrogels (Figure S1, Video S4). Sporozoites were immobile in all hydrogels cured at room temperature (~22°C), regardless of the concentration (Video S5). Collagen fiber

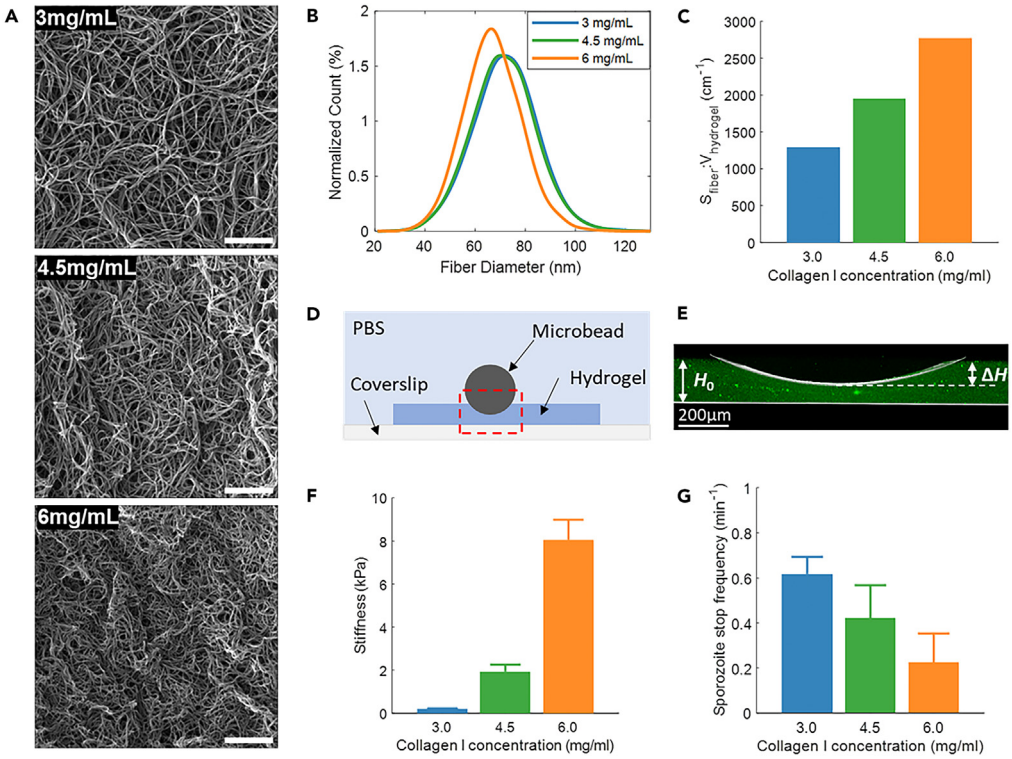

Figure 2. Quantification of the collagen I fiber microstructure and hydrogel stiffness

(A) SEM images of dehydrated collagen I hydrogels of different concentrations. Scale bar: 2 μm.

(B) Collagen fiber diameter distribution from CT-FIRE analysis on the SEM images.

(C) Fiber surface area per unit hydrogel volume in collagen hydrogels of different concentrations.

(D) Schematic showing the indentation measurement for hydrogel stiffness. Measurements were performed in the region marked by the red square.

(E) The x-z view of an overlaid image of fluorescence and reflectance signals of collagen I hydrogel during indentation measurement. The hydrogel is decorated with green fluorescent nanoparticles, and the surfaces of the coverslip and microbead are demarcated in white.

(F) Stiffness of collagen hydrogels at different concentrations. $n = 3$.

(G) Frequency of sporozoite stops during the period of 3D image acquisition. Stops are defined as the duration in which sporozoites have a speed lower than 0.15 μm/s, significantly lower than gliding motility speed.

organizations were imaged using interference reflectance microscopy (IRM), and among those cured at 37°C, visually we observed that the 1.5 mg/mL hydrogels exhibited a low fiber density. Hydrogels cured at room temperature all formed sparse fiber clusters, including the ones cured using the highest concentration of 6 mg/mL (Figure S2). We note that in those hydrogels, while the density within the fiber clusters was high, the spacing between clusters was relatively large, resulting in low local fiber density between fiber clusters where sporozoites moved. Taken together, we conclude that local availability of collagen (i.e., fiber density) is an important parameter for sporozoite motility. Low local fiber densities observed in gels consisting of 1.5 mg/mL collagen or those cured at room temperature resulted in immobility or detachment. Therefore, we used collagen I hydrogels at concentrations of 3, 4.5, and 6 mg/mL, cured at 37°C for the subsequent sporozoite motility measurements in the rest of the study.

To quantitatively determine the relationship between collagen hydrogel fiber structure and sporozoite motility, we imaged hydrogels of various collagen densities using scanning electron microscopy (SEM). Upon visual inspection, we observed that higher collagen concentration corresponded to higher fiber density (Figure 2A). We next employed CT-FIRE,[31] an algorithm that automatically extracts fibers from SEM images, to quantify the fiber diameter. This showed that collagen hydrogels at 6 mg/mL hydrogels have an average fiber diameter of 66.7 nm, slightly thinner than hydrogels prepared at 3 and 4.5 mg/mL, whose average fiber diameters were 71.5 and 71.0 nm, respectively (Figure 2B). Given that the dry density of collagen is 1.3 g/cm^3,[32] the fiber surface area per unit volume of hydrogel could be estimated:

$$S_{fiber} : V_{hydrogel} = \frac{c}{\rho \cdot \left(\frac{\pi}{4} D^2\right)} \cdot \pi D \qquad \text{(Equation 1)}$$

where c is the collagen concentration, ρ is the collagen dry density, and D is the fiber diameter. The S_{fiber}:$V_{hydrogel}$ ratio was higher at higher collagen concentrations, matching our qualitative assessment based on IRM images (Figure 2C). Therefore, the S_{fiber}:$V_{hydrogel}$ ratio is a suitable metric of local fiber availability to migrating sporozoites.

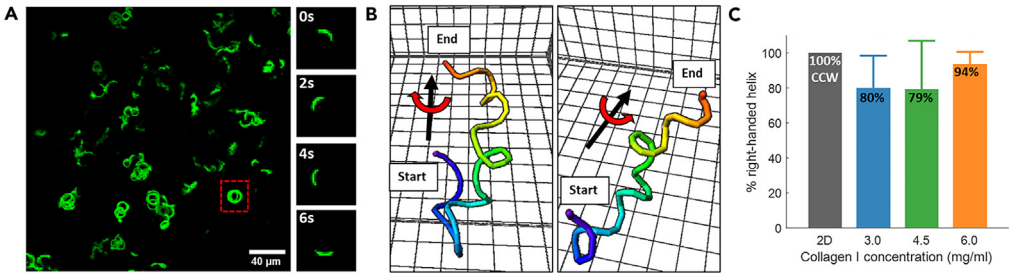

Figure 3. Chirality of sporozoite motility

(A) Maximum intensity projection of sporozoite on collagen-coated glass over time. (Right) The sporozoite indicated with the red box moving counterclockwise.
(B) Examples of left-handed (left) and right-handed (right) helical trajectories of sporozoites in collagen hydrogels. The tracks are color-coded with time.
(C) The chirality of sporozoites on 2D surfaces and in hydrogels of different concentrations are shown. We note that the chirality in 2D was determined by inspecting the 2D movies acquired by an inverted microscope. Sample size: $N_{2D} = 33$, $N_{3.0} = 39$, $N_{4.5} = 37$, $N_{6.0} = 29$. CCW, counterclockwise.

In addition, we measured the stiffness of hydrogels, which is known to also change with collagen concentrations.[33] Based on the microbead indentation measurement (Figures 2D and 2E),[34] the stiffness of 3, 4.5, and 6 mg/mL hydrogels was 0.20 $\pm$ 0.02, 1.94 $\pm$ 0.32, and 8.06 $\pm$ 0.93 kPa (Figure 2F). The stiffness of 6 mg/mL hydrogels was comparable to the average Young's modulus of human skin dermis,[35,36] thus providing physiologically representative information. As collagen concentration decreased, the stiffness decreased significantly. We note that both S_{fiber}:$V_{hydrogel}$ and stiffness values of hydrogels associated with different collagen concentrations exhibited an inverse trend relative to the stop frequencies of sporozoites (Figure 2G). These results suggest that the local availability of collagen and/or the hydrogel stiffness are important for the 3D motility of sporozoites. Further investigations are required to decouple the two factors and their separate contribution on sporozoite migration.

Sporozoite gliding trajectories are dominantly right-handed helices

We proceeded with characterizing the sporozoite gliding motility pattern on 2D surfaces and in 3D collagen gels of various fiber organizations. On 2D surfaces, we observed that sporozoites move in counterclockwise circles (Figures 3A and 3B, Video S6) in agreement with previous studies.[26,51] Next, we examined how such chirality is manifested when sporozoites are placed in physiologically representative 3D microenvironments. We acquired time-lapse z stack images of moving sporozoites in hydrogels and analyzed the 3D trajectories. We found that sporozoites move forward in a distinct helical path. Next, we evaluated how well the trajectories conform to a left-handed or right-handed helix, known as chirality. Helical motion is right-handed when the path of motion along the helix's axis moves toward the observer following a counterclockwise direction. We note that the trajectories were not perfect helices, and we sometimes detected slight deflection in the helix axis. Sometimes the velocity varied from one turn to the next, too. Therefore, we quantified chirality by calculating the percentage of their time moving in the right-handed helix as a percentage of the duration of observation (see the STAR Methods section for details). Both left-handed and right-handed helical trajectories could be seen in sporozoite motility (Figure 3B). Between the two motility modes, right-handed helical motion is dominant in all conditions tested. Specifically, sporozoites followed right-handed helical trajectories ~80% of the time in 3 and 4.5 mg/mL collagen hydrogels and 94% in 6 mg/mL collagen hydrogels (Figure 3C). The chirality in 2D was determined by inspecting the 2D movies acquired by an inverted microscope, following the previously established protocol for analyzing the trajectories of sporozoites moving on 2D surface. Expectedly, our results agreed with the previous studies where 2D sporozoite migration was imaged using an inverted microscope and exhibited dominantly counterclockwise motion.[37]

Sporozoites show lower speed but faster dissemination in dense hydrogel (6.0 mg/mL) compared to others

Sporozoites are known to undergo stick-and-slip shuffles when gliding on 2D surfaces. To examine whether this pattern is conserved in 3D migration, we calculated the instantaneous speed of sporozoites over time, based on the reconstructed 3D trajectories. Consistent with previous studies, we found that sporozoites alternate between fast and slow phases on collagen-I-coated glass surfaces, with the slow phase 50%–70% slower than the fast phase. Inside collagen gels, although the instantaneous speed of sporozoites still exhibited fast and slow phases, the difference between the two phases was much smaller, where the slow phase was only 10%–20% slower than the fast phase (Figure 4A). This is also reflected in the normalized distribution of the instantaneous speed, which shows a smaller spread for sporozoites in collagen gels (Figure 4B).

Next, we quantified the magnitude of sporozoite speed. We found that on average, sporozoites moved at 2 μm/s in 3 and 4.5 mg/mL hydrogels. However, in 6 mg/mL hydrogels, the magnitude of the moving speed was significantly lower, at 1.7 μm/s (Figure 4C). It is widely accepted that the high speed of sporozoites is the key to efficient dissemination from the injection sites into the dermal tissue *in vivo*. Therefore, we measured the dissemination of sporozoites in physiologically representative collagen hydrogels by calculating the mean squared displacement (MSD) over time (Figure 4D). A steeper slope of the MSD curve signifies faster dissemination. Interestingly, sporozoites disseminated much faster in 4.5 mg/mL and 6 mg/mL hydrogels compared to 3 mg/mL hydrogels, contrary to the trend observed in the instantaneous speed. By fitting the MSD curves to the diffusion model [$\langle r^2(\tau)\rangle = K_\alpha \tau^\alpha$], we found that in 4.5 mg/mL and 6 mg/mL hydrogels,

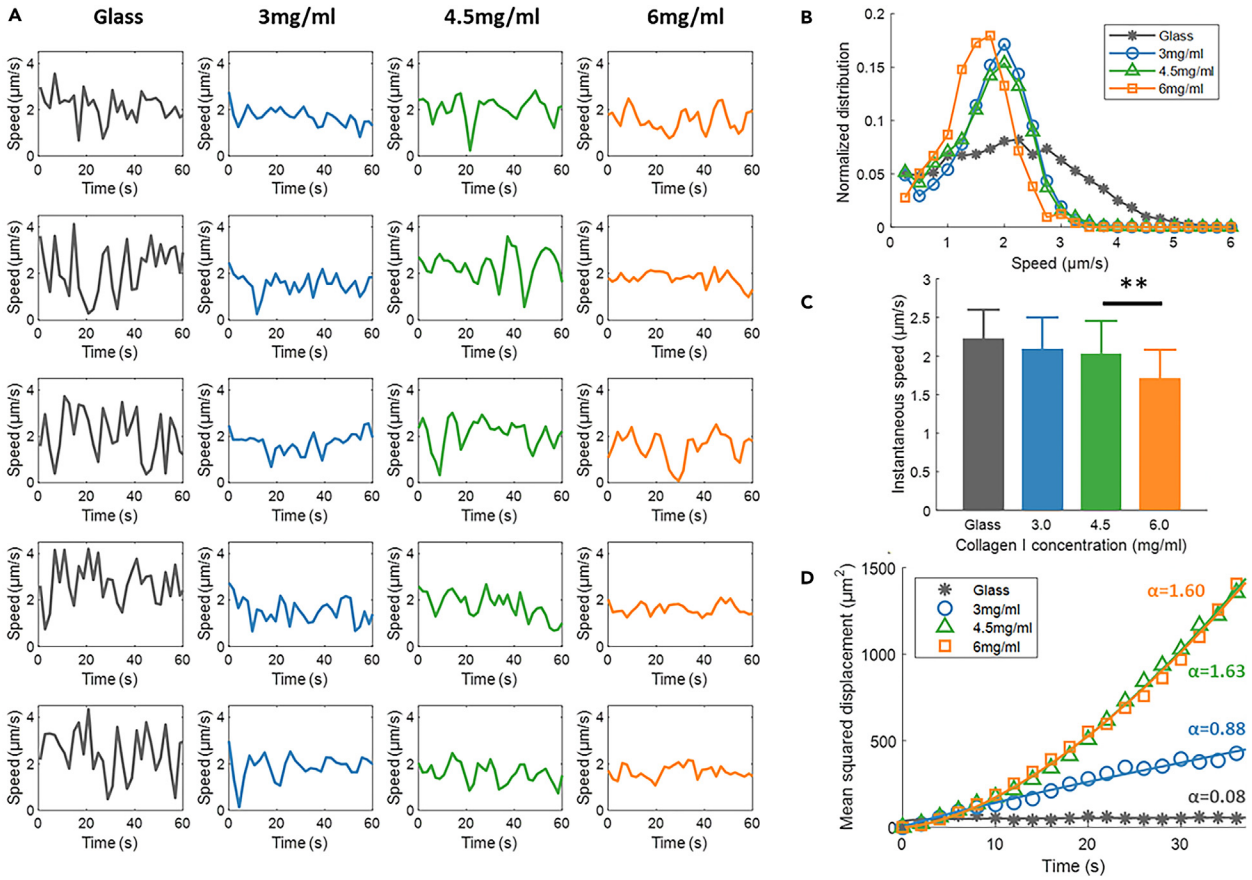

Figure 4. Speed patterns of sporozoites in collagen I hydrogels and on collagen-I-coated glass surfaces

(A) Exemplary instantaneous speed curves of sporozoites on collagen-coated glass surfaces (first column), in 3 mg/mL second column), 4.5 mg/mL (third column), and 6 mg/mL (fourth column) collagen I hydrogels.

(B) Distribution of the instantaneous speed of sporozoites.

(C) Average instantaneous speed of sporozoites. *$p < 0.05$, **$p < 0.01$, ***$p < 0.001$, ****$p < 0.0001$, ns., not significant. The error bar indicates the standard deviation. This applies to other figures unless stated otherwise.

(D) Mean squared displacement of sporozoites. The markers show the measured result, and the solid lines show the fitting to the diffusion model [$\langle r^2(\tau)\rangle = K_\alpha \tau^\alpha$], with the power α indicated.

sporozoites are in a superdiffusive state, where the power α is 1.63 and 1.60, respectively. This means the sporozoites have more rapid dissemination than the rate of Brownian motion ($\alpha = 1$). In comparison, sporozoites in 3 mg/mL hydrogels are in a subdiffusive state ($\alpha = 0.88$).

Sporozoites follow straighter trajectories in denser hydrogels

Next, we sought the explanation for the observation that sporozoites disseminate faster at high collagen concentration, despite lower magnitudes of average speed. As sporozoites follow helical trajectories, their dissemination is affected by both the shape of each helical loop and the overall directionality of the helix axis. First, we parameterized the shape of each helical loop by calculating the radius of the helix, as well as the forward displacement of the sporozoite after completing one loop (pitch). We found that higher collagen concentrations correlated with larger pitch lengths (Figure 5A) and the radius became smaller (Figure 5B). On the other hand, examining the time required for sporozoites to complete one helical loop (period) revealed that no significant difference existed between the three concentrations (Figure 5C). The change in the shape of helical loops is illustrated in Figure 5E. Second, to analyze the directionality of the axis of helix, we used the coordinates of sporozoites after completing each helical loop as an approximation for the axis (Figure S6). Then we calculated the straightness of the axis and found that it is higher in high-concentration collagen gels (Figure S3). Together with the fact that the pitch became larger, and the radius became smaller, our observation indicates that the linearity of the trajectory increased with the collagen concentration (Figure 5D). In other words, at higher collagen concentration, sporozoites moved in a straighter and narrower helical trajectory. We concluded that the straighter trajectories contributed to faster dissemination at higher collagen concentrations. In addition, we crosslinked 3 mg/mL collagen hydrogels using genipin to increase their stiffness by 20-fold while not affecting the fiber density. We found that it did not drastically change the sporozoite motility (Figure S4), suggesting ECM stiffness plays a minor role in modulating sporozoite motility.

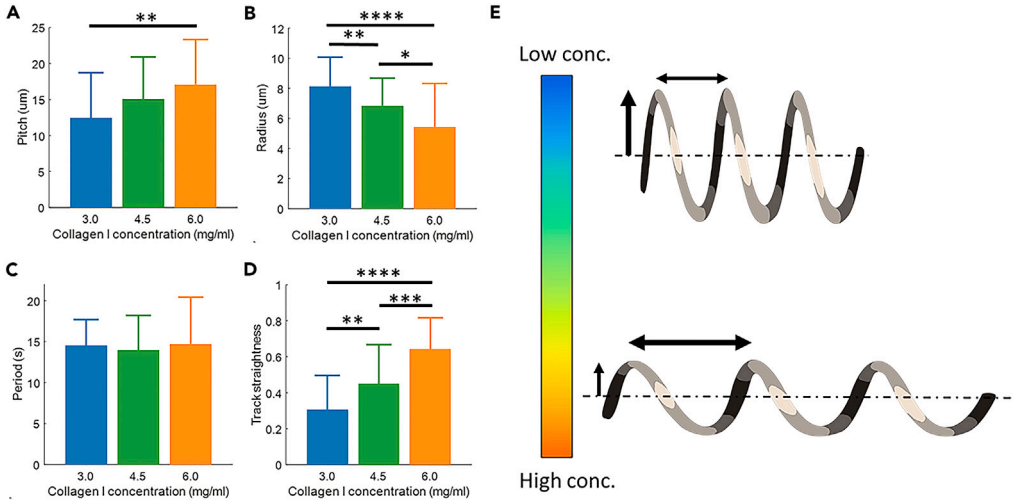

Figure 5. Parameterization of the helical pattern of sporozoite gliding motility

(A–D) Pitch, radius, period, and track straightness of sporozoite helical trajectories in collagen hydrogels of different concentrations.

(E) The helical pattern changes along with collagen concentration.

DISCUSSION

In this study, we conducted the first-ever characterization of sporozoite motility in 3D. The 3D trajectories recorded here provided a more realistic picture than 2D tracking regarding how sporozoites move. Taking into account their movement in the z direction, the measured speed was more informative of what occurs in physiological conditions (Figure S5). Our experimental and analytical pipeline is a useful addition to the toolbox for studying sporozoite gliding motility.[38] Moreover, several interesting findings made here may inspire future studies.

First, we found that the speed and linearity of the sporozoite motility also changed as a function of collagen concentration. This implies that sporozoites are equipped with adaptability to move in different environments. Several previous studies had shown that the sporozoite motility *in vivo* is location dependent, such as rat tail vs. ear[10] or near vs. away from blood vessels.[25] Collagen concentrations differ from each other in these locations. Our results suggest that, among many variables pertaining to different tissue contexts, indeed ECM concentration, or ECM availability, can be an important factor in modulating sporozoite motility. Specifically, our results aligned well with a recent study, which described two states of sporozoite motility: (1) low-speed, circular-moving, subdiffusive state 1 close to blood vessels, and (2) high-speed, forward-moving, superdiffusive state 2 far from blood vessels. The similarity is obvious if we compare the two states with motility in 3 and 6 mg/mL gels in our results, in terms of the track linearity and dispersion. Intermediate behaviors exist between the two states, just as we have shown with 4.5 mg/mL gels. The speed for state 1 is significantly lower than typical sporozoite motility, which we suspect is a result of sporozoites stopping more often. If that is the case, it again aligned with our finding of higher stop frequency in 3 mg/mL gels. In another related study, Hellmann et al. studied sporozoites in micro-fabricated pillar arrays and found that as they varied the substrate design such as the pillar-to-pillar distance, the trajectory and speed of sporozoites changed accordingly.[25] This along with our findings indicates that without additional biochemical cues, sporozoites are able to adapt to their physical surroundings by varying their moving parameters.

Second, we found that sporozoites demonstrated a right-handed chirality in their helical trajectories. In another study, Kan et al. showed that *P. berghei* ookinetes mostly moved in left-handed helices.[28] Ookinetes and sporozoites are different stages of plasmodium parasites, and they differ a lot in terms of morphology, movement speed, etc. However, it is still striking to see that they showed completely different chirality. It would be interesting to further investigate the determinant of the chirality and find out what causes the switch.

The new insights from our study open the door to a few interesting future directions. For example, Vanderberg found that sporozoites of *P. berghei*, *Plasmodium cynomolgi*, and *Plasmodium falciparum* each have distinct moving patterns *in vivo*, and even *P. berghei* sporozoites from oocysts and from salivary glands move differently.[39] To quantify the motility characteristics resulting in these distinct moving patterns sporozoite across species or across developmental stages, collagen hydrogels are suitable *in vitro* models.

Our study also has limitations. For example, Korne et al. found that syringe-injected sporozoites had slower migration and decreased infectivity in mice, which was likely due to the alteration of dermal tissues by the injection of fluid.[4] We also observed that close to the injection sites there were areas filled with fluids but devoid of collagen fibers, possibly caused by the mechanical impact of needle injection. To better mimic the much gentler process of a mosquito bite causing negligible ECM alterations, in future studies microneedles should be employed for injection, or real mosquitos should be used to inoculate sporozoites. Moreover, although collagen I is the main component of the dermal ECM, it is not the only component. A more comprehensive hydrogel model should be established, which includes other components such as fibronectin and collagen IV, to develop a better mimicry of the skin tissue mechanically and biochemically. This hydrogel model might serve as a screening tool for the effect of malaria prophylactics and drugs on sporozoite motility,[14,40] which will be more physiologically relevant than 2D assays and less cumbersome than *in vivo* studies. We note that the stiffness measurement based on indentation by beads can only survey the

stiffness of the sample in a relatively coarse manner. The heterogeneity in elastic moduli across the collagen hydrogel could not be mapped using this method. Our rationale to choose this method of bulk measurement was based on the fact that migrating sporozoites were not confined in specific local regions. Rather, their trajectories covered a vast volume of hydrogel. Therefore, measuring the bulk stiffness was appropriate, providing information regarding the trend of how sporozoites migrate in hydrogels of various collagen densities. Although there is heterogeneity within the same collagen hydrogel, it is widely agreed that hydrogels consisting of higher density of collagen are stiffer than those of lower density. Moreover, the values of the bulk stiffness measured here agree with atomic force microscopy (AFM) measurement results reported previously.[41] Importantly, the stiffness of the collagen hydrogels used in our study matched the stiffness of the dermis in the human skin.[42] Our observations are thus physiologically relevant.

It should be noted that ookinetes and sporozoites of the same species have opposite handedness.[28] Furthermore, ookinetes also move at a much slower speed (0.1 μm/s)[28] compared to the sporozoites (3 μm/s).[8] One possible reason might be that ookinetes and sporozoites are different morphologies, which are known as an important parameter contributing to migration speed and orientation.[43]

Conclusions

In summary, we demonstrated that collagen I hydrogel is a suitable *in vitro* 3D model to study sporozoite motility. The 3D imaging and tracking technique employed in the study allowed us to gain new knowledge about sporozoite gliding motility. We found that sporozoites moved in right-handed helices, and in hydrogels of higher concentrations, sporozoites disseminated faster despite lower speed, due to straighter trajectories. Three-dimensional *in vitro* models are an important tool to investigate sporozoite motility, and a deeper understanding of how they migrate in the dermis is a crucial step in the development of malaria vaccines and drugs targeting the skin stage.

Limitations of the study

We acknowledge that sporozoites could have more motility modes in 3D environments than those described in the current study. For example, while frequent rotations, as in a helical trajectory, are characteristic of sporozoite motility in the skin, sometimes they can also move in a very linear manner without a change of direction.[44] A deeper, mechanistic understanding is required to explain why and how they transition between different motility modes. While studies have shown the crucial involvement of thrombospondin-related anonymous protein (TRAP) family adhesins[45–47] and actomyosin motors,[48,49] there is yet to be a holistic model to integrate these factors governing sporozoite motility. With this model, we can investigate how sporozoites move when they lack or express low levels of sporozoite surface proteins like TRAP. Another application of the simplified model described here will be in the evaluation of antibodies targeting sporozoites. Sporozoites, when deposited in the skin by mosquitoes, must move swiftly and find the blood vessels in order to infect hepatocytes. Antibodies that target sporozoite motility have been shown to effectively prevent liver stage infection.[13,15] A simplified model recapitulating skin physiology will be critical for screening potential vaccines and/or monoclonal antibodies targeted to inhibit sporozoite motility.

STAR★METHODS

Detailed methods are provided in the online version of this paper and include the following:

- KEY RESOURCES TABLE
- RESOURCE AVAILABILITY
  - Lead contact
  - Materials availability
  - Data and code availability
- EXPERIMENTAL MODEL AND STUDY PARTICIPANT DETAILS
  - Mice
  - Parasites
  - Mosquito
- METHOD DETAILS
  - Preparation of collagen I hydrogels
  - *Plasmodium berghei* mCherry sporozoites
  - Sporozoite motility assay preparation
  - Confocal imaging
  - Calculation of sporozoite stop frequency
  - Sporozoite tracking
  - Parameterization of sporozoite helical trajectory
  - SEM imaging and analysis
  - Hydrogel stiffness measurement
- QUANTIFICATION AND STATISTICAL ANALYSIS

SUPPLEMENTAL INFORMATION

Supplemental information can be found online at https://doi.org/10.1016/j.isci.2024.110463.

ACKNOWLEDGMENTS

We thank the team of the parasitology and insectary core facilities at the Johns Hopkins Malaria Research Institute at the Bloomberd School of Public Health and Bloomberg Philanthropies for their support for these facilities. We thank Photini Sinnis and Sachie Kanatani for helpful discussion and technical assistance. This work was supported by a pilot grant from Johns Hopkins Malaria Research Institute at the Bloomberd School of Public Health to I.B., A.K.T., and Y.C.

AUTHOR CONTRIBUTIONS

Conceptualization, A.K.T., Y.C., and I.B.; methodology, A.K.T., Y.C., and I.B.; investigation, Z.L., S.L., P.A., T.T., L.W., J.C., and Y.C.; formal analysis, Z.L., S.L., P.A., T.T., L.W., J.C., and R.T.; writing—original draft, Z.L., A.K.T., Y.C., and I.B.; writing—review & editing, R.T. and Y.C.; funding acquisition, A.K.T., Y.C., and I.B.; supervision, A.K.T., Y.C., and I.B.

DECLARATION OF INTERESTS

The authors declare no competing interests.

Received: September 28, 2023
Revised: November 20, 2023
Accepted: July 2, 2024
Published: July 5, 2024

REFERENCES

1. World Health Organization. (2022). World Malaria Report 2022. Global report
2. Frischknecht, F., Baldacci, P., Martin, B., Zimmer, C., Thiberge, S., Olivo-Marin, J.-C., Shorte, S.L., and Ménard, R. (2004). Imaging movement of malaria parasites during transmission by Anopheles mosquitoes: Imaging Plasmodium sporozoites in mosquito salivary glands. Cell Microbiol. *6*, 687–694. https://doi.org/10.1111/j.1462-5822.2004.00395.x.
3. Vaughan, J.A., Davis, J.R., Beier, M.S., Beier, J.C., and Noden, B.H. (1991). Quantitation of Plasmodium falciparum Sporozoites Transmitted in Vitro by Experimentally Infected Anopheles gambiae and Anopheles stephensi. Am. J. Trop. Med. Hyg. *44*, 564–570. https://doi.org/10.4269/ajtmh.1991.44.564.
4. De Korne, C.M., Winkel, B.M.F., Van Oosterom, M.N., Chevalley-Maurel, S., Houwing, H.M., Sijtsma, J.C., Azargoshasb, S., Baalbergen, E., Franke-Fayard, B.M.D., Van Leeuwen, F.W.B., and Roestenberg, M. (2021). Clustering and Erratic Movement Patterns of Syringe-Injected versus Mosquito-Inoculated Malaria Sporozoites Underlie Decreased Infectivity. mSphere *6*, e00218. https://doi.org/10.1128/mSphere.00218-21.
5. Medica, D.L., and Sinnis, P. (2005). Quantitative Dynamics of *Plasmodium yoelii* Sporozoite Transmission by Infected Anopheline Mosquitoes. Infect. Immun. *73*, 4363–4369. https://doi.org/10.1128/IAI.73.7.4363-4369.2005.
6. Beier, J.C., Onyango, F.K., Koros, J.K., Ramadhan, M., Ogwang, R., Wirtz, R.A., Koech, D.K., and Roberts, C.R. (1991). Quantitation of malaria sporozoites transmitted in vitro during salivation by wild Afrotropical Anopheles. Med. Vet. Entomol. *5*, 71–79. https://doi.org/10.1111/j.1365-2915.1991.tb00523.x.
7. Yamauchi, L.M., Coppi, A., Snounou, G., and Sinnis, P. (2007). Plasmodium sporozoites trickle out of the injection site. Cell Microbiol. *9*, 1215–1222. https://doi.org/10.1111/j.1462-5822.2006.00861.x.
8. Amino, R., Thiberge, S., Martin, B., Celli, S., Shorte, S., Frischknecht, F., and Ménard, R. (2006). Quantitative imaging of Plasmodium transmission from mosquito to mammal. Nat. Med. *12*, 220–224. https://doi.org/10.1038/nm1350.
9. Hopp, C.S., and Sinnis, P. (2015). The innate and adaptive response to mosquito saliva and *Plasmodium* sporozoites in the skin. Ann. N. Y. Acad. Sci. *1342*, 37–43. https://doi.org/10.1111/nyas.12661.
10. Hopp, C.S., Chiou, K., Ragheb, D.R., Salman, A.M., Khan, S.M., Liu, A.J., and Sinnis, P. (2015). Longitudinal analysis of Plasmodium sporozoite motility in the dermis reveals component of blood vessel recognition. Elife *4*, e07789. https://doi.org/10.7554/eLife.07789.
11. Sinnis, P., and Zavala, F. (2012). The skin: where malaria infection and the host immune response begin. Semin. Immunopathol. *34*, 787–792. https://doi.org/10.1007/s00281-012-0345-5.
12. Matsuoka, H., Yoshida, S., Hirai, M., and Ishii, A. (2002). A rodent malaria, Plasmodium berghei, is experimentally transmitted to mice by merely probing of infective mosquito, Anopheles stephensi. Parasitol. Int. *51*, 17–23. https://doi.org/10.1016/S1383-5769(01)00095-2.
13. Vanderberg, J.P., and Frevert, U. (2004). Intravital microscopy demonstrating antibody-mediated immobilisation of Plasmodium berghei sporozoites injected into skin by mosquitoes. Int. J. Parasitol. *34*, 991–996. https://doi.org/10.1016/j.ijpara.2004.05.005.
14. Douglas, R.G., Reinig, M., Neale, M., and Frischknecht, F. (2018). Screening for potential prophylactics targeting sporozoite motility through the skin. Malar. J. *17*, 319. https://doi.org/10.1186/s12936-018-2469-0.
15. Aliprandini, E., Tavares, J., Panatieri, R.H., Thiberge, S., Yamamoto, M.M., Silvie, O., Ishino, T., Yuda, M., Dartevelle, S., Traincard, F., et al. (2018). Cytotoxic anti-circumsporozoite antibodies target malaria sporozoites in the host skin. Nat. Microbiol. *3*, 1224–1233. https://doi.org/10.1038/s41564-018-0254-z.
16. Flores-Garcia, Y., Nasir, G., Hopp, C.S., Munoz, C., Balaban, A.E., Zavala, F., and Sinnis, P. (2018). Antibody-Mediated Protection against *Plasmodium* Sporozoites Begins at the Dermal Inoculation Site. mBio *9*, e02194-18. https://doi.org/10.1128/mBio.02194-18.
17. Aguirre-Botero, M.C., Wang, L.T., Formaglio, P., Aliprandini, E., Thiberge, J.-M., Schön, A., Flores-Garcia, Y., Mathis-Torres, S., Flynn, B.J., Da Silva Pereira, L., et al. (2023). Cytotoxicity of human antibodies targeting the circumsporozoite protein is amplified by 3D substrate and correlates with protection. Cell Rep. *42*, 112681. https://doi.org/10.1016/j.celrep.2023.112681.
18. Frénal, K., Dubremetz, J.-F., Lebrun, M., and Soldati-Favre, D. (2017). Gliding motility powers invasion and egress in Apicomplexa. Nat. Rev. Microbiol. *15*, 645–660. https://doi.org/10.1038/nrmicro.2017.86.
19. Kappe, S.H.I., Buscaglia, C.A., Bergman, L.W., Coppens, I., and Nussenzweig, V. (2004). Apicomplexan gliding motility and host cell invasion: overhauling the motor model. Trends Parasitol. *20*, 13–16. https://doi.org/10.1016/j.pt.2003.10.011.
20. Menard, R. (2001). Gliding motility and cell invasion by Apicomplexa: insights from the Plasmodium sporozoite. Microreview. Cell. Microbiol. *3*, 63–73. https://doi.org/10.1046/j.1462-5822.2001.00097.x.
21. Yahata, K., Hart, M.N., Davies, H., Asada, M., Wassmer, S.C., Templeton, T.J., Treeck, M., Moon, R.W., and Kaneko, O. (2021). Gliding motility of *Plasmodium* merozoites. Proc. Natl. Acad. Sci. *118*, e2114442118. https://doi.org/10.1073/pnas.2114442118.
22. Ripp, J., Kehrer, J., Smyrnakou, X., Tisch, N., Tavares, J., Amino, R., Ruiz De Almodovar, C., and Frischknecht, F. (2021). Malaria parasites differentially sense environmental elasticity during transmission. EMBO Mol. Med. *13*,

e13933. https://doi.org/10.15252/emmm.202113933.
23. Meissner, M., Ferguson, D.J., and Frischknecht, F. (2013). Invasion factors of apicomplexan parasites: essential or redundant? Curr. Opin. Microbiol. *16*, 438–444. https://doi.org/10.1016/j.mib.2013.05.002.
24. Formaglio, P., Wosniack, M.E., Tromer, R.M., Polli, J.G., Matos, Y.B., Zhong, H., Raposo, E.P., Da Luz, M.G.E., and Amino, R. (2023). Plasmodium sporozoite search strategy to locate hotspots of blood vessel invasion. Nat. Commun. *14*, 2965. https://doi.org/10.1038/s41467-023-38706-z.
25. Hellmann, J.K., Münter, S., Kudryashev, M., Schulz, S., Heiss, K., Müller, A.-K., Matuschewski, K., Spatz, J.P., Schwarz, U.S., and Frischknecht, F. (2011). Environmental Constraints Guide Migration of Malaria Parasites during Transmission. PLoS Pathog. *7*, e1002080. https://doi.org/10.1371/journal.ppat.1002080.
26. Kudryashev, M., Münter, S., Lemgruber, L., Montagna, G., Stahlberg, H., Matuschewski, K., Meissner, M., Cyrklaff, M., and Frischknecht, F. (2012). Structural basis for chirality and directional motility of *Plasmodium* sporozoites: Chirality of *Plasmodium* sporozoites. Cell Microbiol. *14*, 1757–1768. https://doi.org/10.1111/j.1462-5822.2012.01836.x.
27. Amino, R., Giovannini, D., Thiberge, S., Gueirard, P., Boisson, B., Dubremetz, J.-F., Prévost, M.-C., Ishino, T., Yuda, M., and Ménard, R. (2008). Host Cell Traversal Is Important for Progression of the Malaria Parasite through the Dermis to the Liver. Cell Host Microbe *3*, 88–96. https://doi.org/10.1016/j.chom.2007.12.007.
28. Kan, A., Tan, Y., Angrisano, F., Hanssen, E., Rogers, K.L., Whitehead, L., Mollard, V.P., Cozijnsen, A., Delves, M.J., Crawford, S., et al. (2014). Quantitative analysis of *P lasmodium* ookinete motion in three dimensions suggests a critical role for cell shape in the biomechanics of malaria parasite gliding motility. Cell Microbiol. *16*, 734–750. https://doi.org/10.1111/cmi.12283.
29. Winkel, B.M.F., De Korne, C.M., Van Oosterom, M.N., Staphorst, D., Bunschoten, A., Langenberg, M.C.C., Chevalley-Maurel, S.C., Janse, C.J., Franke-Fayard, B., Van Leeuwen, F.W.B., and Roestenberg, M. (2019). A tracer-based method enables tracking of *Plasmodium falciparum* malaria parasites during human skin infection. Theranostics *9*, 2768–2778. https://doi.org/10.7150/thno.33467.
30. Yang, Y., Motte, S., and Kaufman, L.J. (2010). Pore size variable type I collagen gels and their interaction with glioma cells. Biomaterials *31*, 5678–5688. https://doi.org/10.1016/j.biomaterials.2010.03.039.
31. Bredfeldt, J.S., Liu, Y., Pehlke, C.A., Conklin, M.W., Szulczewski, J.M., Inman, D.R., Keely, P.J., Nowak, R.D., Mackie, T.R., and Eliceiri, K.W. (2014). Computational segmentation of collagen fibers from second-harmonic generation images of breast cancer. J. Biomed. Opt. *19*, 016007. https://doi.org/10.1117/1.JBO.19.1.016007.
32. O'Brien, F.J., Harley, B.A., Yannas, I.V., and Gibson, L.J. (2005). The effect of pore size on cell adhesion in collagen-GAG scaffolds. Biomaterials *26*, 433–441. https://doi.org/10.1016/j.biomaterials.2004.02.052.
33. Joshi, J., Mahajan, G., and Kothapalli, C.R. (2018). Three-dimensional collagenous niche and azacytidine selectively promote time-dependent cardiomyogenesis from human bone marrow-derived MSC spheroids. Biotechnol. Bioeng. *115*, 2013–2026. https://doi.org/10.1002/bit.26714.
34. Gross, W., and Kress, H. (2017). Simultaneous measurement of the Young's modulus and the Poisson ratio of thin elastic layers. Soft Matter *13*, 1048–1055. https://doi.org/10.1039/C6SM02470J.
35. Chen, A.I., Balter, M.L., Chen, M.I., Gross, D., Alam, S.K., Maguire, T.J., and Yarmush, M.L. (2016). Multilayered tissue mimicking skin and vessel phantoms with tunable mechanical, optical, and acoustic properties. Med. Phys. *43*, 3117–3131. https://doi.org/10.1118/1.4951729.
36. Zahouani, H., Pailler-Mattei, C., Sohm, B., Vargiolu, R., Cenizo, V., and Debret, R. (2009). Characterization of the mechanical properties of a dermal equivalent compared with human skin *in vivo* by indentation and static friction tests. Skin Res. Technol. *15*, 68–76. https://doi.org/10.1111/j.1600-0846.2008.00329.x.
37. Patra, P., Beyer, K., Jaiswal, A., Battista, A., Rohr, K., Frischknecht, F., and Schwarz, U.S. (2022). Collective migration reveals mechanical flexibility of malaria parasites. Nat. Phys. *18*, 586–594. https://doi.org/10.1038/s41567-022-01583-2.
38. Carey, A.F., Ménard, R., and Bargieri, D.Y. (2012). Scoring Sporozoite Motility. In Malaria, R. Ménard, ed. (Humana Press), pp. 371–383. https://doi.org/10.1007/978-1-62703-026-7_26.
39. Vanderberg, J.P. (1974). Studies on the Motility of *Plasmodium* Sporozoites. J. Protozool. *21*, 527–537. https://doi.org/10.1111/j.1550-7408.1974.tb03693.x.
40. De Korne, C.M., Van Schuijlenburg, R., Sijtsma, J.C., De Bes, H.M., Baalbergen, E., Azargoshasb, S., Van Oosterom, M.N., McCall, M.B.B., Van Leeuwen, F.W.B., and Roestenberg, M. (2022). Sporozoite motility as a quantitative readout for anti-CSP antibody inhibition. Sci. Rep. *12*, 17194. https://doi.org/10.1038/s41598-022-22154-8.
41. Doyle, A.D., Carvajal, N., Jin, A., Matsumoto, K., and Yamada, K.M. (2015). Local 3D matrix microenvironment regulates cell migration through spatiotemporal dynamics of contractility-dependent adhesions. Nat. Commun. *6*, 8720. https://doi.org/10.1038/ncomms9720.
42. Park, S., Tao, J., Sun, L., Fan, C.-M., and Chen, Y. (2019). An Economic, Modular, and Portable Skin Viscoelasticity Measurement Device for In Situ Longitudinal Studies. Molecules *24*, 907. https://doi.org/10.3390/molecules24050907.
43. Bodor, D.L., Pönisch, W., Endres, R.G., and Paluch, E.K. (2020). Of Cell Shapes and Motion: The Physical Basis of Animal Cell Migration. Dev. Cell *52*, 550–562. https://doi.org/10.1016/j.devcel.2020.02.013.
44. Winkel, B.M.F., De Korne, C.M., Van Oosterom, M.N., Staphorst, D., Meijhuis, M., Baalbergen, E., Ganesh, M.S., Dechering, K.J., Vos, M.W., Chevalley-Maurel, S.C., et al. (2019). Quantification of wild-type and radiation attenuated Plasmodium falciparum sporozoite motility in human skin. Sci. Rep. *9*, 13436. https://doi.org/10.1038/s41598-019-49895-3.
45. Beyer, K., Kracht, S., Kehrer, J., Singer, M., Klug, D., and Frischknecht, F. (2021). Limited Plasmodium sporozoite gliding motility in the absence of TRAP family adhesins. Malar. J. *20*, 430. https://doi.org/10.1186/s12936-021-03960-3.
46. Boucher, L.E., Hopp, C.S., Muthinja, J.M., Frischknecht, F., and Bosch, J. (2018). Discovery of *Plasmodium* (M)TRAP–Aldolase Interaction Stabilizers Interfering with Sporozoite Motility and Invasion. ACS Infect. Dis. *4*, 620–634. https://doi.org/10.1021/acsinfecdis.7b00225.
47. Song, G., Koksal, A.C., Lu, C., and Springer, T.A. (2012). Shape change in the receptor for gliding motility in *Plasmodium* sporozoites. Proc. Natl. Acad. Sci. *109*, 21420–21425. https://doi.org/10.1073/pnas.1218581109.
48. Ripp, J., Smyrnakou, X., Neuhoff, M., Hentzschel, F., and Frischknecht, F. (2022). Phosphorylation of myosin A regulates gliding motility and is essential for *Plasmodium* transmission. EMBO Rep. *23*, e54857. https://doi.org/10.15252/embr.202254857.
49. Bane, K.S., Lepper, S., Kehrer, J., Sattler, J.M., Singer, M., Reinig, M., Klug, D., Heiss, K., Baum, J., Mueller, A.-K., and Frischknecht, F. (2016). The Actin Filament-Binding Protein Coronin Regulates Motility in Plasmodium Sporozoites. PLoS Pathog. *12*, e1005710. https://doi.org/10.1371/journal.ppat.1005710.
50. Sundararaghavan, H.G., Monteiro, G.A., Lapin, N.A., Chabal, Y.J., Miksan, J.R., and Shreiber, D.I. (2008). Genipin-induced changes in collagen gels: Correlation of mechanical properties to fluorescence. J. Biomed. Mater. Res. *87*, 308–320. https://doi.org/10.1002/jbm.a.31715.
51. De Korne, C.M., Lageschaar, L.T., Van Oosterom, M.N., Baalbergen, E., Winkel, B.M.F., Chevalley-Maurel, S.C., Velders, A.H., Franke-Fayard, B.M.D., Van Leeuwen, F.W.B., and Roestenberg, M. (2019). Regulation of Plasmodium sporozoite motility by formulation components. Malar. J. *18*, 155. https://doi.org/10.1186/s12936-019-2794-y.
52. Münter, S., Sabass, B., Selhuber-Unkel, C., Kudryashev, M., Hegge, S., Engel, U., Spatz, J.P., Matuschewski, K., Schwarz, U.S., and Frischknecht, F. (2009). Plasmodium Sporozoite Motility Is Modulated by the Turnover of Discrete Adhesion Sites. Cell Host Microbe *6*, 551–562. https://doi.org/10.1016/j.chom.2009.11.007.
53. Stein, A.M., Vader, D.A., Jawerth, L.M., Weitz, D.A., and Sander, L.M. (2008). An algorithm for extracting the network geometry of three-dimensional collagen gels. J. Microsc. *232*, 463–475. https://doi.org/10.1111/j.1365-2818.2008.02141.x.
54. Plotnikov, S.V., Sabass, B., Schwarz, U.S., and Waterman, C.M. (2014). High-Resolution Traction Force Microscopy. In Methods in Cell Biology (Elsevier), pp. 367–394. https://doi.org/10.1016/B978-0-12-420138-5.00020-3.

STAR★METHODS

KEY RESOURCES TABLE

REAGENT or RESOURCE	SOURCE	IDENTIFIER
Chemicals, peptides, and recombinant proteins		
Genipin	Sigma-Aldrich, Sundararaghavan et al.[50]	Cat# 6902-77-8
collagen I rat tail	Corning, Yang et al.[30]	Cat# 354236
Hexamethyldisilazane	Fisher Scientific	Cat# AAA15139AC
glutaraldehyde	Millipore Sigma	Cat# G7776
Experimental models: organisms/strains		
P. berghei mCherry-UIS4	Hopp et al.,[10] JHMRI Parasite core	https://publichealth.jhu.edu/malaria-research-institute/research/core-facilities/parasitology-core-facility
Swiss Webster mice	Taconic	RRID: IMSR_TAC:SW
A. stephensi mosquitoes	JHMRI insectary core	https://publichealth.jhu.edu/malaria-research-institute/research/core-facilities/insectary-core-facility
Software and algorithms		
Imaris	Imaris	https://imaris.oxinst.com/
MATLAB (R2023a)	Mathworks	https://matlab.mathworks.com/
CT-FIRE V2.0 Beta	Laboratory for Optical and Computational Instrumentation, Bredfeldt et al.,[31] Stein et al.[53]	https://loci.wisc.edu/ctfire/
ImageJ	NIH	https://imagej.net/ij/
Other		
Beads: Borosilicate	Winsted Precision Ball	Cat# 3200940F1ZZ00A0
Beads: polystyrene	Cospheric	Cat# DMB-RWHT-1.38
Beads: Fluorescent nanobeads	Invitrogen	Cat# F10720

RESOURCE AVAILABILITY

Lead contact

Further information and requests for resources and reagents should be directed to and will be fulfilled by the lead contact, Yun Chen (yun.chen@jhu.edu).

Materials availability

This study did not generate new unique reagents.

Data and code availability

- All relevant data is available in the main text and supplemental information. Any additional information can be provided upon reasonable request to the authors.
- This paper does not report the original code.
- Any additional information required to reanalyze the data reported in this paper is available from the lead contact upon request.

EXPERIMENTAL MODEL AND STUDY PARTICIPANT DETAILS

Mice

Swiss Webster mice were purchased from Taconic (Germantown, NY). All animal studies were conducted under a protocol (MO20H05) approved by the Johns Hopkins Animal Care and Use Committee. Experimental animals were housed in cages shared by three mice. 6-8 week-old female mice were randomly assigned to experimental groups.

Parasites

The parasites used in this study were P. berghei mCherry-UIS4, which was generated as previously described by Hopp and colleagues.[10]

Mosquito

The mosquitoes used in this study were A. stephensi mosquitoes to feed on infected mice. Infected mosquitoes were maintained for up to 25 days at 18°C with 80% humidity and provided a 10% (w/v) sucrose solution.

METHOD DETAILS

Preparation of collagen I hydrogels

Similar to a previously described protocol,[30] collagen I hydrogels were prepared using ~9.5 mg/mL high concentration collagen I rat tail stock solution (Corning). Appropriate amounts of the stock solution were mixed with HPLC water and 10% (v/v of the final solution) 10x PBS to reach the desired concentrations of 3, 4.5, and 6 mg/mL 0.5M NaOH was added dropwise until the pH reached 7.4. All the solutions were kept on ice to prevent gelation during mixing. 80μL of the hydrogel solution was added to each well of an 18-well chambered cover glass (Cellvis), and adjacent wells were filled with PBS to prevent the solution from drying out. The collagen solution was then transferred immediately into a 37°C incubator, and hydrogels were formed after 3-h incubation. To further crosslink the collagen hydrogel, we followed the protocol developed by Sundararaghavan et al.[50] Briefly, 150 μL 1mM genipin (Sigma-Aldrich) in PBS was added on top of the hydrogel and incubated at 37°C for 12 h. Afterward, the genipin solution was removed, and the hydrogel was washed with PBS three times before being stored at room temperature.

Plasmodium berghei mCherry sporozoites

Mosquito infection with *P. berghei* mCherry-UIS4 was performed as previously described.[10] Swiss Webster mice (Taconic, Germantown, NY) were infected with *P. berghei* mCherry-UIS4 parasites, and once abundant gametocyte-stage parasites were observed, *A. stephensi* mosquitoes (3–7 days after emergence) were allowed to feed on infected mice. Infected mosquitoes were maintained for up to 25 days at 18°C with 80% humidity and were provided with a 10% (w/v) sucrose solution.

Sporozoite motility assay preparation

To extract live sporozoites, the mosquitoes were dissected 23–24 days after infection, and the obtained salivary glands were homogenized in RPMI 1640 (Corning Cellgro) supplemented with 10% fetal bovine serum (FBS, Corning Cellgro), 100U/mL penicillin and 100U/mL streptomycin (Corning Cellgro). The homogenized solution was kept on ice and used within 1 h. As bovine serum albumin (BSA) was found to be an essential supplement for sporozoite motility,[51] an equal volume of 2% BSA (Sigma-Aldrich) and the homogenized solution were mixed and incubated at 37°C for 5.5 min to activate the sporozoites. For 2D motility assays, the solution was added onto a collagen I-coated 384-well microplate (Greiner Bio) and spun down at 200G for 5min. For 3D motility assays, the solution (2000 spz/ul) was injected into previously prepared hydrogels using a 1mL syringe and 26G needle (BD). Sporozoites were imaged within 1.5 h after activation.

Confocal imaging

A confocal microscope with both fluorescence and reflectance modes (Leica TCS SP8) was used to acquire time-lapse z stack images of sporozoites moving in hydrogels. A 40x/1.1 NA water-immersion objective was used. Imaging was performed at 30°C to maintain the activity of sporozoites. The red fluorescence emitted by mCherry was detected to record the trajectories of sporozoites. z stack images were acquired over time with the sporozoites of interest centered in the field of view. To reconcile the tradeoff between image quality and sampling rate, each frame contained 10–12 stacks at 5μm intervals, and the resolution for each stack was 128 × 128 pixels, with the pixel size of 1.14 μm/pixel. The resulting acquisition rate was ~0.5Hz per frame. The 3D movies were acquired until either the sporozoite moved out of the field of view, or a maximum of 200 frames was reached. Then, the IRM images (1024 × 1024 pixels) were acquired at the same location to survey the fine collagen fiber organization in the presence of and visualize collagen fibers.

Calculation of sporozoite stop frequency

Calculation of the stop frequency of sporozoites was based on the assumption that sporozoites making stops during gliding motility follows a Poisson distribution. Then the frequency can be calculated as:

$$f = \frac{N_{stop}}{T_{total} - T_{stop}}$$

where N_{stop} is the total number of stops observed in all the acquired sporozoite tracks in one set of experiments, T_{total} is the sum of all the track durations, and T_{stop} is the sum of the durations of all the stops. Stops are defined as a period of time during which the sporozoite has a speed lower than 0.15 μm/s. At least three independent repeat experiments were performed on each condition. Then, the final average and standard deviation were calculated, weighted by the number of tracks in each repeat experiment.

Sporozoite tracking

The trajectories of sporozoites were extracted using the Imaris software. First, the image files acquired from the confocal microscope were converted using the Imaris File Converter. Within Imaris, sporozoites were identified using the Surface model. The threshold was manually adjusted if necessary to filter out background noise while recognizing the entirety of the sporozoite. Then tracking was done with the autoregressive motion algorithm. The created track was then visually inspected, and manual edits were made in the following cases: (1) if the sporozoite touched the boundary of the field of view, most often at the end of the video, those few frames were deleted; (2) if sporozoites were incorrectly identified in a few frames, such as two sporozoites recognized as one when they moved close to each other, the tracks were manually corrected frame by frame. After editing, the following statistics for each track were output for further analysis: position, displacement, speed, time, and track straightness.

Parameterization of sporozoite helical trajectory

In addition to the metrics directly acquired from Imaris, the following were calculated, which were specific to the helical nature of the sporozoite trajectories: chirality, radius, pitch, and period. The calculation was done in MATLAB.

The chirality of sporozoites was quantified by calculating the percentage of the time they migrate in right-handed helices. This is done by averaging the local chirality for all the time points in one track. Local chirality is a binary number, 0 or 1, and was calculated based on the instantaneous speed of three adjacent time points, i.e., $\boldsymbol{V}(t)$, $\boldsymbol{V}(t+1)$, $\boldsymbol{V}(t+2)$. If the angle between $\boldsymbol{V}(t+2)$ and the cross product of $\boldsymbol{V}(t)$ and $\boldsymbol{V}(t+1)$, $\angle\,(\boldsymbol{V}(t) \times \boldsymbol{V}(t+1), \boldsymbol{V}(t+2))$, is smaller than $\pi/2$, then the helix is right-handed, and number 1 is assigned. If it is larger than $\pi/2$, then the helix is left-handed, and number 0 is assigned. After calculating the local chirality for all the time points in a track, i.e., $t = 0, 1, 2, \ldots, T\text{-}2$, an average was taken, and the result, ranging between 0 and 1, represents the % right-handed helix in the track.

The period is defined as the time it takes for the sporozoite to complete one helical loop. Assuming t_0 is the starting timepoint, then the period is T at the first local minimum of $\angle\,(\boldsymbol{V}(t_0), \boldsymbol{V}(t_0+T))$. Then t_0+T is used as the next starting timepoint to iteratively calculate the next period. An example is shown in Figure S6.

Pitch is defined as the forward displacement of the sporozoite after one helical loop. It was calculated as the distance between the locations before and after one period, $\|\boldsymbol{L}(t_0+T) - \boldsymbol{L}(t_0)\|$.

The radius of the helix was calculated as the maximal distance away from the starting point when projected along the forward movement direction of the helix. In each track, a radius was calculated for each completed helical loop, and an average of all the radii was calculated for the track.

SEM imaging and analysis

Before SEM imaging, prepared collagen I hydrogels were subjected to fixation and serial dehydration. Hydrogels were first fixed with 2.5% glutaraldehyde (Millipore Sigma) for 12 h. Then, they were washed three times with PBS and twice with HPLC water, for 5 min per wash. After washing, hydrogels were dehydrated using a series of water and ethanol mixtures with ascending concentrations of ethanol (30%, 50%, 70%, 90%, 100%), for 10 min each. Then, they were dehydrated using a series of ethanol and hexamethyldisilazane (HMDS, Fisher Scientific) mixtures with ascending concentrations for HMDS (30%, 50%, 70%, 90%, 100%), for 15 min each. Next, each hydrogel was transferred onto an SEM sample stub and kept at room temperature for an additional 2 h for further drying. Then, the hydrogels mounted onto stubs were sputter coated with Au/Pd to a thickness of 5nm using a Leica EM ACE600 high vacuum sputter coater.

After sample preparation, the hydrogels were imaged at 20kV and 27.7kx magnification using a Tescan Mira3 Scanning Electron Microscope. The images obtained had a view field of 10μm. 20 images were obtained on each sample, and the measurement was repeated on three independent samples.

Finally, fiber diameter analysis was done on the SEM images using CT-FIRE V2.0 Beta. This software uses discrete curvelet transform to denoise the image and enhance fiber edge features and uses a fiber extraction (FIRE) algorithm to extract individual fibers and calculate fiber diameter.[31,53]

Hydrogel stiffness measurement

The stiffness of collagen hydrogels was measured using a microbead indentation method.[34] Borosilicate (Winsted Precision Ball, 3200940F1ZZ00A0) or polystyrene (Cospheric, DMB-RWHT-1.38) beads were placed on top of previously prepared collagen I hydrogels and allowed at least 15 min to deform the collagen hydrogel before measurements were taken. The microbeads and collagen hydrogel were completely immersed in PBS throughout the measurement. Fluorescent nanobeads (Invitrogen, F10720) were mixed with collagen solution at 1:20000 concentration as fiducial markers to visualize the indentation. Previous studies have shown the addition of fluorescent nanobeads at low concentrations does not significantly alter the hydrogel stiffness.[54] Collagen hydrogels were imaged on a confocal microscope (Leica SP8). Stiffness values were calculated with custom codes in MATLAB (Mathworks, R2023a).

To obtain the elastic modulus, the force applied to the collagen was calculated. ρ_{ball} is the borosilicate or polystyrene density, ρ_{PBS} is the density of the PBS solution, and r is the ball radius:

$$F = \frac{4}{3}\pi r^3(\rho_{ball} - \rho_{PBS})$$

Indentation depth δ and hydrogel thickness h were then measured from images of indented collagen hydrogel. Briefly, the xz-slice where the microbead was at its lowest position in the whole stack was used for measurement. This slice represents the center of the bead. Three horizontal lines were drawn at the top of the hydrogel, the bottom of the microbead (tangential to the microbead), and the bottom of the dish. Indentation depth δ was the distance from the top of the hydrogel to the bottom of the microbead, and hydrogel thickness h was the distance from the top of the hydrogel to the bottom of the dish. Image processing was performed in ImageJ (NIH, 1.53t). Poisson's ratio ν was assumed to be 0.5 for collagen hydrogel. Correction terms α, β, χ, C were then calculated as previously described[33]:

$$\alpha = -\frac{1.2876 - 1.4678\nu + 1.3442\nu^2}{1-\nu}$$

$$\beta = \frac{0.6387 - 1.0277\nu + 1.5164\nu^2}{1-\nu}$$

$$\chi = \frac{\sqrt{r\delta}}{h}$$

$$C = 1 - 2\alpha\frac{\chi}{\pi} + 4\alpha^2\frac{\chi^2}{\pi^2} - \left(8\alpha^3 + \frac{32}{15}\pi^2\beta\right)\frac{\chi^3}{\pi^3} + \left(16\alpha^4 + \frac{48}{5}\pi^2\beta\right)\frac{\chi^4}{\pi^4}$$

Finally, the elastic modulus E was estimated by:

$$E = \frac{3(1-\nu^2)F}{4C\sqrt{r\delta^3}}$$

QUANTIFICATION AND STATISTICAL ANALYSIS

For the analysis of sporozoite track speed, straightness, pitch, radius, and period, statistical significance was determined using a two-sample t-test. Statistical significance was set at $p < 0.05$. The data were expressed in the figures as mean $\pm$ deviation.